Classification of Remote Sensing Images with Parametrized Quantum Gates

Soronzonbold Otgonbaatar, Mihai Datcu, *Fellow, IEEE*

***Abstract*—This paper studies how to program and assess a Parametrized Quantum Circuit (PQC) for classifying Earth observation (EO) satellite images. In this exploratory study, we assess a PQC for classifying a two-label EO image dataset and compare it with a classic deep learning classifier. We use the PQC with an input space of only 17 quantum bits (qubits) due to the current limitations of quantum technology. As a real-world image for EO, we selected the Eurosat dataset obtained from multispectral Sentinel-2 images as a training dataset and a Sentinel-2 image of Berlin, Germany as a test image. However, the high dimensionality of our images is incompatible with the PQC input domain of 17 qubits. Hence, we had to reduce the dimensionality of the input images for this two-label case to a vector with 16 elements; the 17th qubit remains reserved for storing label information. We employed a Very Deep Convolutional Network with an autoencoder as a technique for the dimensionality reduction of the input image, and we mapped the dimensionally-reduced image onto 16 qubits by means of parameter thresholding. Then, we used a PQC to classify the two-label content of the dimensionally-reduced Eurosat image dataset. A PQC classifies the Eurosat images with high accuracy as a classic deep learning method (and with even better accuracy in some instances). From our experiment, we derived and enhanced deeper insight into programming future gate-based quantum computers for many practical problems in EO.**

***Index Terms*—Parametrized Quantum Circuit, Quantum Machine Learning, Earth observation.**

I. Introduction

MACHINE Learning (ML) is a framework of methods to extract underlying features and patterns from heterogeneous big data. By learning features or a probability distribution of patterns in the dataset, one can perform tasks such as prediction, clustering, or data classifications in hitherto unknown domains. Such ML tasks are elements of supervised and unsupervised learning methods. A supervised learning method has to learn about conditional probability information of the dataset given its correct labels, e.g., classification and prediction [1]. The training of a labeled dataset is a classic example of supervised learning, and can be done with high validation accuracy [2]. In contrast, an unsupervised learning method deals with the datasets which do not yet have label information, e.g., results generated by clustering. Deep learning is a heuristic method which can be composed of several layers with artificial neurons [3] in which the connections of each layer are parametrized, while the parameters are tuned by using loss functions. Typical examples include Hopfield networks (HNs) and Boltzmann Machines (BMs) [4], which are related to an Ising-type model. BMs have artificial neurons with set of values $\{-1, +1\}$, while HNs have a continuous set of values. In practical applications, BMs are often intractable due to their high-dimensional dataset. This difficulty can be overcome by a Restricted Boltzmann Machine.

Authors are with German Aerospace Center (DLR), Oberpfaffenhofen.
E-mail: soronzonbold.otgonbaatar@dlr.de, mihai.datcu@dlr.de.

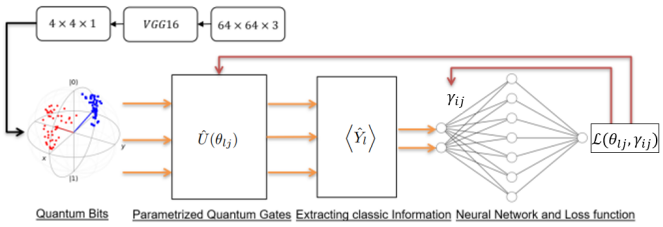

Fig. 1. A hybrid network, a classic and a Parametrized Quantum Circuit layer where θ_{lj}, γ_{ij} are training parameters.

A Restricted Boltzmann Machine (RBM) is composed of two layers named hidden $\mathbf{h}$ and visible $\mathbf{v}$. The hidden and visible layers form a bipartite graph which provides connections between the layers but not within the layers $\mathbf{v} \overset{p(h|v)}{\longleftrightarrow} \mathbf{h}$. The RBM can be extended with additional hidden layers $\mathbf{h}_1$, and the RBM, now called a deep RBM, then forms the layers as $\mathbf{v} \overset{p(h|v)}{\longleftrightarrow} \mathbf{h} \overset{p(h_1|h)}{\longleftrightarrow} \mathbf{h}_1$. The deep RBM performs better for training the dataset than other deep learning methods [4], and is employed for data encoding, dimensionality reduction, as well as a feature extraction [5].

In addition, Noisy Intermediate-Scale Quantum (NISQ) devices are a novel quantum computing technology providing solutions for sampling from hard-to-simulate probability distributions, e.g., (Restricted) Boltzmann Machines, solving high-complexity problems or supporting machine learning algorithms for the first time [6], [7], [8]. An NISQ device is termed a PQC when it has parametrized quantum gates. Sometimes, the PQC is interchangeable with Quantum Machine Learning (QML). As for multispectral images in Earth observation, deep learning networks can handle big data and are very successful methods for scene classification [9], [10], [11], [12], [13]. More importantly, they are independent of the input size of the multispectral images, and their outputs are continuous values. However, in our case study, the PQC has 16 *qubits as input* (due to the current limitations of the quantum technology), and *a single qubit as output* yielding a binary value depending on the binary state of the qubits. Therefore, we had to focus on how to feed the two-label images of Earth observation into 16 qubits and how to program the parametrized quantum gates of the PQC. As a real-world image dataset of Earth observation, we consider a multispectral Eurosat Sentinel-2 image dataset [14] as a training dataset and

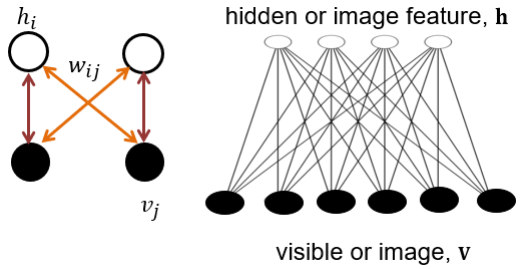

Fig. 2. A Restricted Boltzmann Machine (RBM). An image $\mathbf{v}$ with a size of $64 \times 64 \times 3$ elements is encoded as an another image $\mathbf{h}$ with a size of $4 \times 4 \times 1$.

a real-world Sentinel-2 image of Berlin, Germany, as a test image; each image in this training dataset is a vector with a size of $64 \times 64 \times 3$ elements, and the test image is a vector with a size of $692 \times 633 \times 3$ elements. Therefore, as already mentioned above, there are several challenges when we feed these high-dimensional images to the input space of 16 qubits as well as programming the PQC.

To overcome the challenges above mentioned, we introduce a hybrid (classic-quantum) network which is a combination of a conventional computer and the PQC (Fig. 1). For this hybrid network, we leverage the classic deep learning architecture, a Very Deep Convolutional Network (VGG16) [15], and an autoencoder such as RBM to reduce the dimension of the Eurosat image to a vector with a size of $4 \times 4 \times 1$ elements; in particular, the VGG16 network extracts the most meaningful features of the Eurosat images, and the autoencoder encodes these meaningful features to a vector with a size of $4 \times 4 \times 1$ elements. We then feed these encoded features to the inputs of the PQC. Besides, for programming the PQC, we apply a conventional computer to differentiate the loss function, and to update the trainable parameters of the quantum gates in the PQC [2]. Thus, this study aims for the leveraging of some classic techniques and a conventional computer to support the PQC, and for outlining potential challenges when programming the PQC for a real-world Earth observation dataset.

This paper is structured as follows: In Section II-A, we introduce the dimensionality reduction of the Eurosat image dataset. Then we devise our Parametrized Quantum Circuit for the classification of the dimensionally-reduced images (Section II-B), and in Section III, we benchmark our Parametrized Quantum Circuit for the Eurosat dataset. Finally, we evaluate the developed classification method using the Parametrized Quantum Circuit for a remotely-sensed image of Berlin, Germany, acquired by Sentinel-2 (see Section IV) and draw some conclusions (Section V).

II. Hybrid Network

A. A classic layer for the dimensionality reduction of the Eurosat dataset

We have a hybrid classic-quantum layer, where the classic layer is composed of the VGG16 and the convolutional autoencoder. We use this classic layer for extracting physically meaningful features from the Eurosat image dataset as an RBM. The RBM is capable of encoding the features of the dataset with very few bits. Moreover, the BMs with binary variables are a special type of HNs and represent an energy-based model in terms of an Ising model. Such a model is used to establish a most probable configuration of particles with binary states, and further, the Ising model can be formulated as

$$\begin{aligned} E(\mathbf{v},\mathbf{h}) &= -\sum_i b_i h_i - \sum_i c_j v_j - \sum_{i<j} w_{ij} h_i v_j, \\ P(\mathbf{v},\mathbf{h}) &= \frac{e^{-E(\mathbf{v},\mathbf{h})}}{\sum_{\mathbf{v},\mathbf{h}} E(\mathbf{v},\mathbf{h})}, \quad \mathbf{v},\mathbf{h} \in \mathbb{R}^n; \end{aligned} \tag{1}$$

where b_i, c_j are bias coefficients, and w_{ij} represents the strength of interaction between the neighbour variables v_j and h_i where v_j is called a visible variable in a visible layer, and h_i is called a hidden variable in a hidden layer (see Fig. 2). The probability distribution $P(\mathbf{v},\mathbf{h})$ defines a most probable configuration of the given variables. This formulation is named after an RBM.

To find the most probable configuration of the visible variable, one needs to integrate out (marginalize) hidden variables and then maximize its log-likelihood distribution. Moreover, we represent an input image as the visible layer, and its selected features are represented in the hidden layer (Fig. 2). In other words, we can encode an input image by a very small number of the hidden variables in the hidden layer. This encoding procedure is sometimes called dimensionality reduction or autoencoding of the input image.

B. A quantum layer as a training layer

A quantum circuit is an ensemble of quantum gates and quantum bits, and quantum gates (e.i. unitary operation) operate on quantum bits to perform computations (rotations). A collection of quantum gates with trainable parameters is called a Parametrized Quantum Circuit (PQC). *Quantum gates* are devised as a unitary operation $\hat{U}(\beta)$, which is expressed as follows

$$\hat{U}(\beta) = e^{-i\beta\hat{H}}, \tag{2}$$

where β is a trainable parameter, $\hat{H}$ represents a collection of 2×2 matrices that are named after Pauli matrices, and the Pauli matrices rotate a quantum bit (qubit) to an another quantum bit. *Qubits* are state vectors, and two state vectors or simply two state qubits are $|0\rangle$ and $|1\rangle$, which are bits in a quantum computer.

We are considering a PQC with 17 input qubits. Hence, we first need to make a dimensionality reduction for the Eurosat images since each image is a vector with the high spatial dimensionality of $\mathbf{v} \in \mathbb{R}^{64\times64\times3}$, and second, we encode the dimensionally-reduced images into qubits $|q\rangle = |q_1\rangle\,|q_2\rangle \ldots |q_{16}\rangle\,, \quad |q_j\rangle \in \{|0\rangle\,, |1\rangle\}$ named "data qubits", and their labels $l(\mathbf{v}) \in \{-1, +1\}$ are in 17th qubit $|q_l\rangle = |q_{17}\rangle$ named "readout qubit" (see Fig. 3); this step is called *quantum encoding* [16], [17]. The readout qubit yields either "+1" or "-1" as output. Hence, it is natural to have the two-label Eurosat image data as input image.

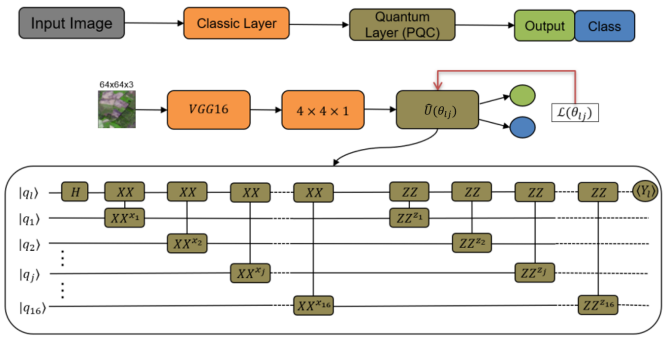

Fig. 3. Top: A general scheme for classifying the Eurosat image dataset, Middle: A detailed scheme for classifying the Eurosat image dataset, Bottom: The architecture of the PQC with inputs of 17 qubits; $|q_l\rangle$ represents a "readout qubit", the other ones are "data qubits". H is a Hadamard matrix, "XX" and "XX^{x_j}" represent $e^{-i\theta^x_{lj}\hat{X}_l\hat{X}_j}$, and $x_j = \theta^x_{lj}$; the same representation is used for "ZZ" and "ZZ^{z_j}" (see Eq. (5)).

Quantum encoding, after the dimensionality reduction of the images, is then the representation of the classic data points $\mathbf{v}$ as quantum states $|q\rangle$. Moreover, we are leveraging the classic layer to extract the physically meaningful 16 features of the Eurosat images, and then we are encoding them in 16 qubits of the PQC (Fig. 3 Top and Middle).

The PQC architecture for the Eurosat image classification task is designed as an energy-based model [2], [18] such that

$$\hat{H} = \sum_j (J^x_{lj}\hat{X}_l\hat{X}_j + J^z_{lj}\hat{Z}_l\hat{Z}_j), \tag{3}$$

where Pauli matrices $\hat{X}_l$ and $\hat{Z}_l$ are representing readout qubit operators, $\hat{X}_j$ and $\hat{Z}_j$ are data qubit operators, and the strength parameters (J^x_{lj}, J^z_{lj}) are among the readout qubit and the data qubit operators.

We then write the unitary operation according to Eq. (2) as

$$\hat{U}(\beta) = e^{-i\beta\hat{H}} = e^{-i\beta\sum_j (J^x_{lj}\hat{X}_l\hat{X}_j + J^z_{lj}\hat{Z}_l\hat{Z}_j)}. \tag{4}$$

By noting $\theta^x_{lj} = \beta J^x_{lj}, \quad \theta^z_{lj} = \beta J^z_{lj}$, we have

$$\hat{U}(\theta_{lj}) = e^{-i\sum_j (\theta^x_{lj}\hat{X}_l\hat{X}_j + \theta^z_{lj}\hat{Z}_l\hat{Z}_j)}, \tag{5}$$

where $(\theta^x_{lj}, \theta^z_{lj})$ are our training parameters (Fig. 3 Bottom). After the unitary operation expressed by Eq. (5) is acted on $|q_j\rangle$, we measure a readout qubit $|q_l\rangle$; the measurement of the readout qubit gives an output, which results from

$$\langle q_l, q_j|\,\hat{U}^\dagger(\theta_{lj})\hat{Y}_l\hat{U}(\theta_{lj})\,|q_j, q_l\rangle = \left\langle \hat{Y}_l \right\rangle, \quad \left\langle \hat{Y}_l \right\rangle \in [-1, +1]. \tag{6}$$

Accordingly, the loss function is then defined by

$$\mathcal{L}(\theta_{lj}) = 1 - l(\mathbf{v})\,\langle q_l, q_j|\,\hat{U}^\dagger(\theta_{lj})\hat{Y}_l\hat{U}(\theta_{lj})\,|q_j, q_l\rangle\,, \tag{7}$$

the parameters of which are updated and optimized by using a conventional computer.

In the next section, we introduce a way to reduce the spatial dimension of each image in the Eurosat dataset into $4 \times 4 \times 1$ elements by preserving their feature information and encoding them into 16 qubits.

Algorithm 1 A hybrid classifier: Classic-Quantum Layer

1: **INPUT:** Eurosat data as training data, and Sentinel-2 image of Berlin, Germany as test data.
2: **OUTPUT:** Generate two-classes.
3: **The dimensionality reduction:** Classic Layer (see Fig. 3):
4: Prepare a VGG16 network with the autonencoder.
5: Encode the Eurosat data and the image of Berlin to $4 \times 4 \times 1$ elements.
6: **Training:** Quantum Layer (see Fig. 3 Bottom):
7: Prepare a PQC layer designed as an energy-based model.
8: Feed dimensionally-reduced Eurosat data to the PQC layer.
9: **Testing:**
10: Feed the dimensionally-reduced image of Berlin to the PQC layer.
11: **STOP ALGORITHM**.

III. Benchmarking the PQC for Earth Observation

The Eurosat dataset is a novel dataset composed of 10 labels and 27,000 geo-referenced images with the RGB spectral bands of the Sentinel-2 satellite (Fig. 4) [14]. Each image within this Eurosat dataset has a size of $64 \times 64 \times 3$ elements and corresponds to a single class. For the classification of this dataset in the PQC, we exploit the hybrid network, namely the classic and the PQC layer (see Fig. 3 and Algorithm 1). The input image to this hybrid network must be the two-label representation of the Eurosat image dataset following the output of the readout qubit in Eq. (6).

The classic layer encodes the two-label images with a size of $64\times64\times3$ elements to ones with a size of $4\times4\times1$ elements, and then it maps these encoded images into 16 input qubits by thresholding them with the value of $\tau = 0.5$; this classic layer is hugely motivated by the RBM autoencoder. The PQC layer is a training layer for the two-label image by means of tuning the parameters of the parametrized quantum gates.

A. Our experiment for Benchmarking the PQC

We designed and implemented our PQC on a classic simulator by using Tensorflow Quantum python kit. One of the important steps to program this PQC is to choose a machinery to feed and embed the classic data into qubits. We had the Eurosat images as our classic data and the classic layer as an autoencoder to feed them to the PQC. Hence, we had to evaluate the performance of the autoencoder for the dimensionality reduction of the Eurosat images. To evaluate its performance, we considered the downsampling technique as well.

For both dimensionality reduction techniques, we classified the dimensionally reduced images on both the PQC and the fully connected classic layer (FCCL) (Fig. 5). We performed this experiment for combinations of binary datasets of the Eurosat images, *Annual Crop and Residential*, *Forest and Highway*, *Forest and Industrial*, and *Herbaceous Vegetation and Residential*.

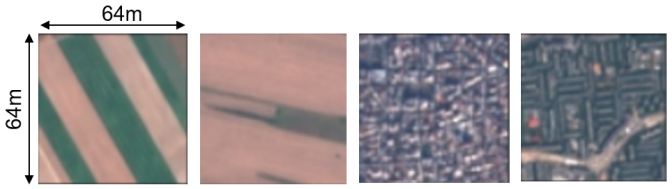

Fig. 4. The Eurosat training image with two labels; *Annual Crop* and *Residential*.

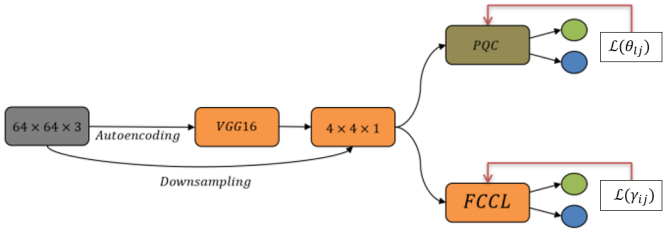

Fig. 5. Graphical representation of the PQC and the classic Fully Connected Classical Layer (FCCL) classification for the Eurosat dataset. The dimension of the images is reduced in two ways, by *autoencoding* and by *downsampling*.

Binary Classifier Accuracy				
	Autoencoding		Downsampling	
Classes	PQC	FCCL	PQC	FCCL
$\{1,2\}$	0.9970	0.9994	0.5575	0.4990
$\{3,4\}$	0.9911	0.9980	0.6230	0.5010
$\{5,6\}$	0.9995	0.9994	0.7123	0.5010
$\{7,8\}$	0.9494	0.9789	0.5258	0.5010

TABLE I
CLASSIFICATION ACCURACY OF THE PQC AND FCCL FOR THE TWO-LABEL REPRESENTATION OF THE EUROSAT IMAGE DATASET. THE DIMENSION OF THE IMAGES IS REDUCED BY AUTOENCODING OR DOWNSAMPLING; $\{i,j\}$ REPRESENT THE TWO CLASSES; $\{1,2\} \rightarrow$ *Annual Crop and Residential*, $\{3,4\} \rightarrow$ *Forest and Highway*, $\{5,6\} \rightarrow$ *Forest and Industrial*, AND $\{7,8\} \rightarrow$ *Herbaceous Vegetation and Residential*.

For the downsampling technique, our experimental results show that the PQC performs better than the FCCL, and it also confirms that the autoencoder is well-suited for reducing the dimensionality of the Eurosat image dataset when compared to the downsampling technique (Table I). Hence, we chose the VVG16 network with the autoencoder for the dimensionality reduction, and we trained the selected hybrid classic-quantum layer for the two-label representation of Eurosat images. Moreover, though the number of qubits is rather limited for the PQC, a classification accuracy of the PQC is even higher than the FCCL in some instances.

These results lead to the conclusion that the PQC could perform even better than conventional classification methods when the number of qubits is increased. In addition, the PQC performance depends on the choice of its optimizer and the depth of the circuit layer, and some care should be taken since the PQC stops a training process due to a vanishing gradient [19]. We experimented on two different optimizers with the Eurosat dataset, namely an *Adam optimizer* and a *Root-Mean-Squared optimizer*. With the *Root-Mean-Squared optimizer*, the PQC stops training the dataset, while the *Adam optimizer* does not terminate.

IV. Validating the PQC with a Sentinel-2 Image of Berlin, Germany

We validated the FCCL and the PQC including its autoencoding with a real-world Sentinel-2 image (Fig. 5); in particular, we considered a Sentinel-2 image of Berlin, Germany, which is not part of the Eurosat images. This Sentinel-2 image consists of multiple classes instead of two classes (Fig. 6 Left). Thus, we classified several scenes of Berlin for different pairs of class combinations (i.e., two-label examples). When we attempted to classify the two-label examples "*Forest and Highway*" and "*Forest and Industrial*", the two classes were identified as a single class, namely "*Forest*", both by the FCCL and the PQC; clearly, the selected Sentinel-2 image of Berlin does not contain the classes "*Highway*" and "*Industrial*". Instead, for the two classes "*Annual Crop and Residential*" and "*Herbaceous Vegetation and Residential*" (Fig. 6 Right), the two-label example is classified as two classes as expected. We visualize these results in Fig. 7. Moreover, these visual results demonstrate that the PQC performs and classifies better for a complex remotely-sensed image than the FCCL.

V. Conclusion

We explored the possible use and challenges encountered with a PQC when handling Earth observation data. More importantly, we assessed the classification performance of a PQC for our Earth observation dataset. First and foremost, we propose a hybrid classic-quantum layer and an autoencoder for dimensionality reduction of Eurosat images. The dimensionality reduction process is even a vital part of classic deep learning methods to reduce the amount of computational effort and to speed up the training process. Second, we encoded the dataset into qubits by thresholding. However, the optimizer has to be chosen wisely to avoid vanishing gradients; we employed an *Adam* optimizer for training the parameters of the PQC. In addition, we attempted to perform a classification of the two-label NWPU-RESISC45 dataset [20]. Unfortunately, the spatial size of these images is too big for the input of the PQC; in particular, a reduced size with 16 elements by exploiting the autoencoder does not result in meaningful features, in contrast to the Eurosat images. As a first step towards assessing and programming the PQC in Earth observation, such big or high-dimensional images are out of scope currently.

We must note however that the proposed method should not viewed as replacements of classical deep learning methods, but our message is that the classical deep learning methods coexist in unity with parametrized quantum circuits (as advocated in our hybrid quantum-classic network). More importantly, a PQC offers invaluable intuition for constructing a physics-aware (based) deep learning method.

Finally, in terms of future work, we will study the dimensionality reduction techniques for high-dimensional images such as NWPU-RESISC45 for a restricted number of inputs of the PQC, and we will then tackle multi-label classification on the PQC.

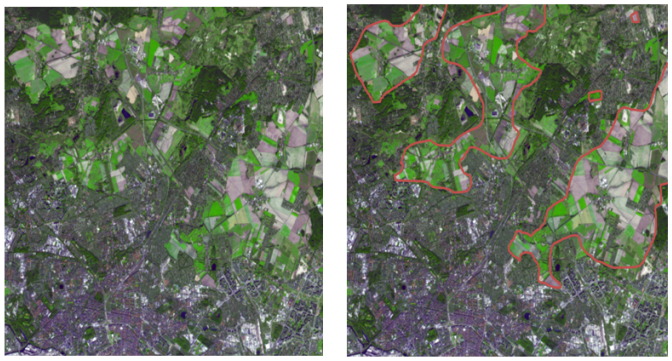

Fig. 6. Left: A Sentinel-2 image of Berlin, Germany, with its RGB spectral band as test image; this test image is not a part of the Eurosat dataset. Right: We visualized a part of Berlin by the *red* contour. The inside of this red contour represents the general class *Vegetation* and *Annual Crop* while the outside represents all other classes. We classified the inside of this red contour by using the FCCL and the PQC.

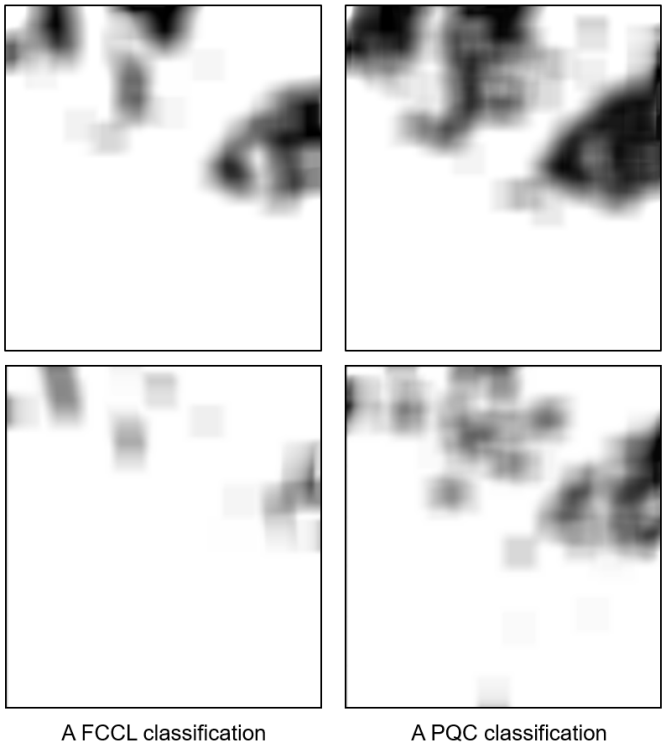

Fig. 7. The FCCL and PQC results for the classification of the test image of Berlin. The visual images show that the PQC is better for detecting vegetation even within built-up areas than a classic FCCL approach. Top: *Annual Crop and Residential*; $White$ denotes the **Residential** class, while $Black$ denotes the **Annual Crop** class. Bottom: *Herbaceous Vegetation and Residential*; $White$ denotes the **Residential** class, while $Black$ denotes the **Herbaceous Vegetation** class.

VI. Acknowledgment

We would like to greatly acknowledge Gottfried Schwarz (DLR, Oberpfaffenhofen) for his valuable comments and contributions to enhance our paper.

References

[1] Y. LeCun, Y. Bengio, and G. Hinton, "Deep learning," *Nature*, vol. 521, no. 7553, pp. 436–444, May 2015. [Online]. Available: https://doi.org/10.1038/nature14539

[2] M. Broughton, G. Verdon, T. McCourt, A. J. Martinez, J. H. Yoo, S. V. Isakov, P. Massey, M. Y. Niu, R. Halavati, E. Peters, M. Leib, A. Skolik, M. Streif, D. V. Dollen, J. R. McClean, S. Boixo, D. Bacon, A. K. Ho, H. Neven, and M. Mohseni, "Tensorflow quantum: A software framework for quantum machine learning," 2020.

[3] A. Krizhevsky, I. Sutskever, and G. E. Hinton, "Imagenet classification with deep convolutional neural networks," *Commun. ACM*, vol. 60, no. 6, p. 84–90, May 2017. [Online]. Available: https://doi.org/10.1145/3065386

[4] R. Salakhutdinov and G. Hinton, "Deep boltzmann machines," in *Proceedings of the Twelth International Conference on Artificial Intelligence and Statistics*, ser. Proceedings of Machine Learning Research, D. van Dyk and M. Welling, Eds., vol. 5. Hilton Clearwater Beach Resort, Clearwater Beach, Florida USA: PMLR, 16–18 Apr 2009, pp. 448–455. [Online]. Available: http://proceedings.mlr.press/v5/salakhutdinov09a.html

[5] M. Küchhold, M. Simon, and T. Sikora, "Restricted boltzmann machine image compression," in *2018 Picture Coding Symposium (PCS)*, 2018, pp. 243–247.

[6] J. Preskill, "Quantum computing in the nisq era and beyond," *Quantum*, vol. 2, p. 79, Aug 2018. [Online]. Available: http://dx.doi.org/10.22331/q-2018-08-06-79

[7] V. Dunjko and H. J. Briegel, "Machine learning & artificial intelligence in the quantum domain: a review of recent progress," *Reports on Progress in Physics*, vol. 81, no. 7, p. 074001, jun 2018. [Online]. Available: https://doi.org/10.1088/1361-6633/aab406

[8] S. Mangini, F. Tacchino, D. Gerace, D. Bajoni, and C. Macchiavello, "Quantum computing models for artificial neural networks," *EPL (Europhysics Letters)*, vol. 134, no. 1, p. 10002, apr 2021. [Online]. Available: https://doi.org/10.1209/0295-5075/134/10002

[9] G. Cheng, X. Xie, J. Han, L. Guo, and G.-S. Xia, "Remote sensing image scene classification meets deep learning: Challenges, methods, benchmarks, and opportunities," *IEEE Journal of Selected Topics in Applied Earth Observations and Remote Sensing*, vol. 13, pp. 3735–3756, 2020.

[10] J. Kang, R. Fernandez-Beltran, Z. Ye, X. Tong, P. Ghamisi, and A. Plaza, "Deep metric learning based on scalable neighborhood components for remote sensing scene characterization," *IEEE Transactions on Geoscience and Remote Sensing*, vol. 58, no. 12, pp. 8905–8918, 2020.

[11] Y. Dong, C. Yang, and Y. Zhang, "Deep metric learning with online hard mining for hyperspectral classification," *Remote Sensing*, vol. 13, no. 7, 2021. [Online]. Available: https://www.mdpi.com/2072-4292/13/7/1368

[12] Y. Dong, T. Liang, Y. Zhang, and B. Du, "Spectral–spatial weighted kernel manifold embedded distribution alignment for remote sensing image classification," *IEEE Transactions on Cybernetics*, vol. 51, no. 6, pp. 3185–3197, 2021.

[13] N. Kussul, M. Lavreniuk, S. Skakun, and A. Shelestov, "Deep learning classification of land cover and crop types using remote sensing data," *IEEE Geoscience and Remote Sensing Letters*, vol. 14, no. 5, pp. 778–782, 2017.

[14] P. Helber, B. Bischke, A. Dengel, and D. Borth, "Eurosat: A novel dataset and deep learning benchmark for land use and land cover classification," *IEEE Journal of Selected Topics in Applied Earth Observations and Remote Sensing*, vol. 12, no. 7, pp. 2217–2226, 2019.

[15] K. Simonyan and A. Zisserman, "Very deep convolutional networks for large-scale image recognition," in *3rd International Conference on Learning Representations, ICLR 2015, San Diego, CA, USA, May 7-9, 2015, Conference Track Proceedings*, Y. Bengio and Y. LeCun, Eds., 2015. [Online]. Available: http://arxiv.org/abs/1409.1556

[16] S. Lloyd, M. Schuld, A. Ijaz, J. Izaac, and N. Killoran, "Quantum embeddings for machine learning," *arXiv:2001.03622*, May 2020. [Online]. Available: https://arxiv.org/abs/2001.03622

[17] M. Schuld and N. Killoran, "Quantum machine learning in feature hilbert spaces," *Phys. Rev. Lett.*, vol. 122, p. 040504, Feb 2019. [Online]. Available: https://link.aps.org/doi/10.1103/PhysRevLett.122.040504

[18] E. Farhi and H. Neven, "Classification with quantum neural networks on near term processors," 2018.

[19] A. Skolik, J. R. McClean, M. Mohseni, P. van der Smagt, and M. Leib, "Layerwise learning for quantum neural networks," *Quantum Machine Intelligence*, vol. 3, no. 1, p. 5, Jan 2021. [Online]. Available: https://doi.org/10.1007/s42484-020-00036-4

[20] G. Cheng, J. Han, and X. Lu, "Remote sensing image scene classification: Benchmark and state of the art," *Proceedings of the IEEE*, vol. 105, no. 10, pp. 1865–1883, 2017.